JOURNAL OF SYNCHROTRON RADIATION

ISSN 1600-5775

Received 9 May 2017
Accepted 18 July 2017

Edited by R. W. Strange, University of Essex, UK

Keywords: *m*-plane; InGaN; XAFS; local structure; step-by-step fitting procedure.

Local structure around In atoms in coherently grown *m*-plane InGaN film

Takafumi Miyanaga,[a]* Takashi Azuhata,[a] Kiyofumi Nitta[b] and Shigefusa F. Chichibu[c]

[a]Department of Mathematics and Physics, Hirosaki University, Hirosaki, Aomori 036-8561, Japan, [b]Japan Synchrotron Radiation Research Institute, Sayo, Hyogo 679-5198, Japan, and [c]Institute of Multidisciplinary Research for Advanced Materials, Tohoku University, Aoba, Sendai 980-8577, Japan. *Correspondence e-mail: takaf@hirosaki-u.ac.jp

The local structure around In atoms in an *m*-plane $In_{0.06}Ga_{0.94}N$ film coherently grown on a freestanding *m*-plane GaN substrate was investigated by polarization-dependent X-ray absorption fine-structure. A step-by-step fitting procedure was proposed for the *m*-plane wurtzite structure. The interatomic distance for the first nearest neighbour In—N atomic pairs was almost isotropic. For the second nearest In—Ga pairs, the interatomic distances along the *m*- and *a*-axes were longer and shorter, respectively, than that in strain-free virtual crystals as expected for the *m*-plane compressive strain. In contrast, the In—Ga interatomic distance in the *c*-direction was elongated in spite of the compressive strain, which was explained in terms of the anisotropic atomic structure on the *m*-plane. The local strain in the *m*-plane film was more relaxed than that in coherently grown *c*-plane single quantum wells. A few In atoms were atomically localized in all directions, and thus localized excitonic emission is expected as in the case of *c*-plane InGaN.

1. Introduction

$In_xGa_{1-x}N$ is a key material in ultraviolet to green light-emitting diodes and laser diodes. Commercially available, such devices have *c*-plane (0001) InGaN quantum wells (QWs) as active layers, where localized excitons contribute to high internal quantum efficiency (Chichibu *et al.*, 1996). The efficiency, however, decreases abruptly due to quantum-confined Stark effects (Chichibu *et al.*, 1996; Takeuchi *et al.*, 1997; Chichibu *et al.*, 2001) for emission wavelengths longer than around 520 nm. The effects are caused by the electrostatic field perpendicular to the QWs due to the piezoelectric and spontaneous polarization (Bernardini & Fiorentini, 1998). In contrast to polar *c*-plane QWs, nonpolar *m*-plane $(1\bar{1}00)$ and *a*-plane $(11\bar{2}0)$ QWs can avoid the quantum-confined Stark effects (Waltereit *et al.*, 2000; Ng, 2002; Kuokstis *et al.*, 2001; Craven *et al.*, 2003; Koida *et al.*, 2004; Onuma *et al.*, 2005) because the polar *c*-axis is parallel to the QW plane. Thus, *m*- and *a*-plane InGaN epilayers are attracting much attention to achieve higher internal quantum efficiency.

In order to make the emission mechanism clear in InGaN-based light-emitting devices, it is important to clarify the local structure around In atoms in active layers. X-ray absorption fine-structure (XAFS) is a powerful tool for investigating local structures in thin layers composed of two or more elements. In particular, polarization-dependent XAFS makes it possible to selectively investigate local structures along specific directions of crystals.

There are many reports on applications of XAFS to InGaN semiconducting films (Blant *et al.*, 1997; Jeffs *et al.*, 1998;

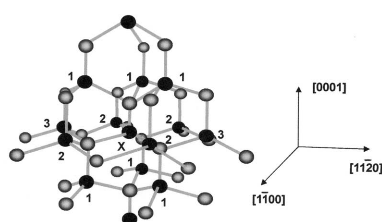

© 2017 International Union of Crystallography

O'Donnell *et al.*, 1999, 2001; Bayliss *et al.*, 1999; Miyajima *et al.*, 2001; Katsikini *et al.*, 2003, 2008; Kachkanov *et al.*, 2006; Sasaki *et al.*, 2007). For *c*-plane InGaN single quantum wells (SQWs), a polarization-dependent extended XAFS (EXAFS) study has been successfully performed and it was suggested that the aggregation of In atoms along the *c*-axis is important for high quantum efficiency in InGaN light-emitting diodes (Miyanaga *et al.*, 2007). As for nonpolar InGaN films, there is no XAFS report and the local structure is still unknown.

In this paper, the results of polarization-dependent In *K*-edge XAFS analyses are reported for an *m*-plane $In_{0.06}Ga_{0.94}N$ film, especially regarding the interatomic distance of the second nearest neighbour (2NN) In—Ga and In—In atomic pairs and the localization of In atoms.

2. Experimental

A 1.5 µm-thick GaN buffer layer and a 300 nm-thick *m*-plane $In_{0.06}Ga_{0.94}N$ film were grown by metalorganic vapour phase epitaxy (MOVPE) on a 325 µm-thick *m*-plane freestanding GaN substrate prepared by halide vapour phase epitaxy. The film was confirmed to be coherently grown on the substrate by an X-ray reciprocal-space mapping method (Chichibu *et al.*, 2008). X-ray absorption measurements were made at the NW10A beamline of the Photon Factory Advanced Ring, KEK. XAFS data were collected with a double-crystal monochromator of Si(311) crystals. Indium K_{α}-fluorescence emission was measured using a 19-element Ge solid-state detector. The incident angle of the X-ray beam to the sample surface was set to be 85°. The following three configurations were used: the electric field vector *E* of the X-ray was parallel to the *c*-axis [0001], the *m*-axis [$1\bar{1}00$] and the *a*-axis [$11\bar{2}0$] as shown in Fig. 1. XAFS data analyses were performed using the *XANADU* code (Sakane *et al.*, 1993) and *FEFF8.10* code (Ankudinov & Rehr, 2000).

3. Results and discussion

Fig. 2 shows atomic structure and crystal axes of the wurtzite structure. The numbers 1, 2 and 3 show three types of atomic positions. Note that the *m*-plane InGaN film is anisotropically strained and that the type 2 atoms and the type 3 atoms are no longer equivalent. Strictly speaking, all the six atoms labelled 1 are not equivalent for the strained wurtzite structure. However, it is quite difficult to analyze them separately owing to too many fitting parameters. Thus, XAFS spectra were analyzed by assuming that the six type 1 Ga/In atoms were equivalent.

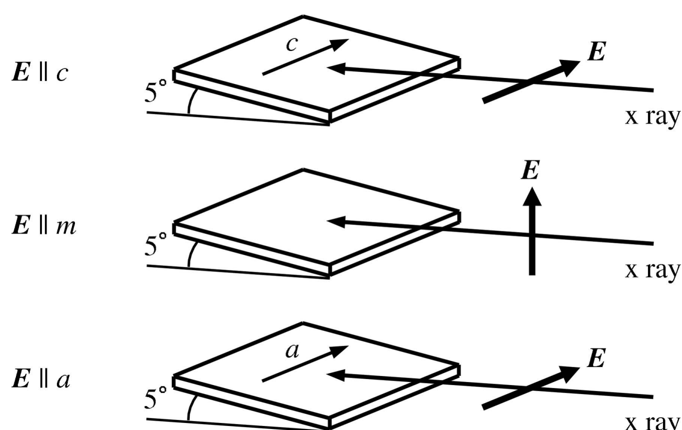

Figure 1
Schematic view of the three configurations used in this study. **E** is the electric field vector of the incident X-rays.

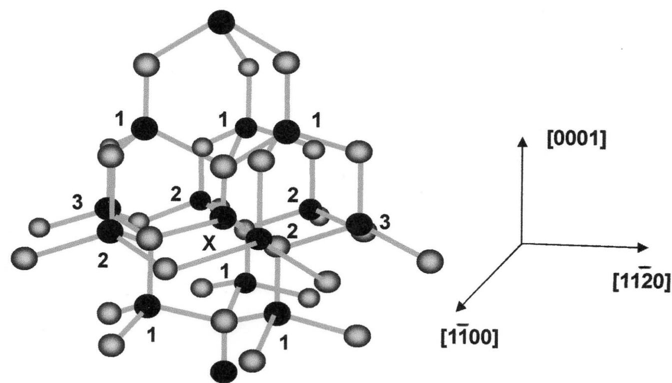

Figure 2
Atomic structure and crystal axes for the model of the *m*-plane $In_{0.06}Ga_{0.94}N$ film. Black circles represent Ga or In atoms and grey ones N atoms. The atom labelled X is the X-ray absorbing In atom and the numbers 1, 2 and 3 show three types of atomic positions.

Fig. 3 shows X-ray absorption near-edge fine structures of the *m*-plane $In_{0.06}Ga_{0.94}N$ film measured in the three configurations. As can be seen from Fig. 3, the structure for $E \parallel c$ is clearly different from those for $E \parallel m$ and $E \parallel a$. This difference is due to the anisotropy of the wurtzite structure and indicates that the dipole-allowed transition probability is smaller for $E \parallel c$ than for $E \parallel m$ and $E \parallel a$. Fig. 4 shows the EXAFS $k\chi(k)$ spectra of the *m*-plane $In_{0.06}Ga_{0.94}N$ film for the three configurations. The data quality is fairly good in the range $k \leq 12.0$ Å^{-1}. Fig. 5 shows the Fourier transforms of the EXAFS data shown in Fig. 4 in the *k*-range 2.0–12.5 Å^{-1}. A clear difference is also found between the $E \parallel c$ data and the others.

To obtain the structural parameters (interatomic distance *r*, coordination number *N* and Debye–Waller factor σ), nonlinear least-square fitting was applied to the EXAFS data.

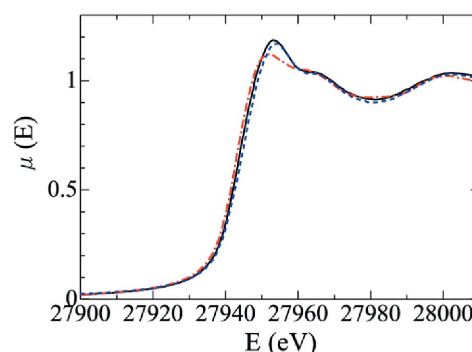

Figure 3
X-ray absorption near-edge structures of the *m*-plane $In_{0.06}Ga_{0.94}N$ film. The red dot-dashed line is for $E \parallel c$, the blue dashed line for $E \parallel m$ and the black solid line for $E \parallel a$.

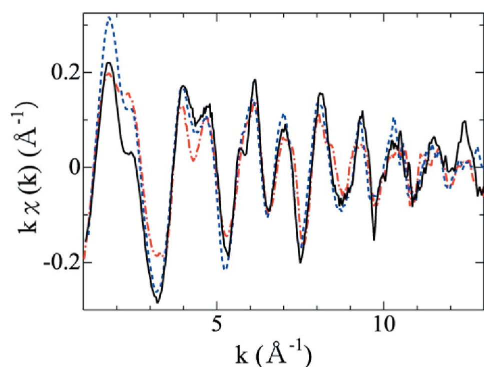

Figure 4
$k\chi(k)$ spectra of the m-plane $In_{0.06}Ga_{0.94}N$ film. The red dot-dashed line is for $E \parallel c$, the blue dashed line for $E \parallel m$ and the black solid line for $E \parallel a$.

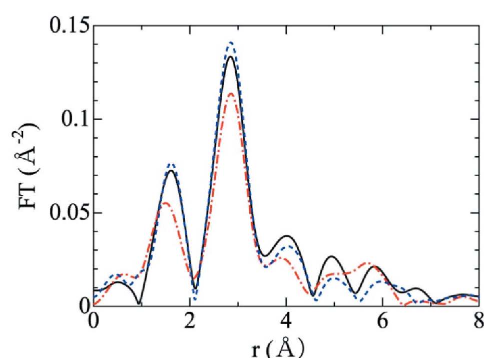

Figure 5
Fourier transforms of the m-plane $In_{0.06}Ga_{0.94}N$ film. The red dot-dashed line is for $E \parallel c$, the blue dashed line for $E \parallel m$ and the black solid line for $E \parallel a$.

Details of the fitting procedure are given elsewhere (Miyanaga *et al.*, 2007). In the present XAFS fitting, the reduction factor was $S_0^2 = 0.9$, and the edge shift from the edge jump was 6.5 eV. The effective coordination number N^* defined as

$$N^* = 3\sum_i \cos^2\theta_i \tag{1}$$

was effectively incorporated into the curve-fitting process. Here, θ_i is the angle between the electric field of the incident X-ray and the direction of the ith photoelectron-scattering atom in the shell from the X-ray absorbing atom. The k-space three-shell fitting in the range 4.0–12.0 $Å^{-1}$ was applied to Fourier-filtered spectra in the r-range from 1.0 to 4.0 Å, in which the contribution from the first nearest neighbour In—N and 2NN In—Ga and In—In atomic pairs are included.

For In—N atomic pairs, $r = 2.10 \pm 0.01$ Å and $N = 4.0 \pm 0.3$ for each direction, indicating that the In—N interatomic distance is almost isotropic. The film is coherently grown on the substrate and is compressively strained. Thus, it is found that the strain-induced change of r for the 2NN In—Ga and In—In atomic pairs is caused by the change of the N—In—N bond angle.

For the analyses of the local structure for 2NN In—Ga and In—In, the following step-by-step procedure was used. First, the $E \parallel c$ data were analyzed. In this configuration, only the type 1 atoms are detected by XAFS. Their effective coordination number N_1^* was set to be 12. The type 2 and 3 atoms are not detected because the plane including these types of atoms and the X-ray absorbing In atom (labelled X in Fig. 2) is perpendicular to E. Thus, N^* for these types of atoms are $N_2^* = N_3^* = 0$. At this first step, r, σ and the ratio $N^*_{\rm In-Ga}/N^*_{\rm In-In}$ for the type 1 atoms were determined.

Second, the $E \parallel m$ data, to which only the type 1 and 2 atoms contribute, were analyzed. Although σ may depend on the polarization direction of the incident X-rays, it was assumed to be isotropic in this study. For r, σ and $N^*_{\rm In-Ga}/N^*_{\rm In-In}$ of the type 1 atoms, the values obtained at the first step were used. N_1^* and N_2^* were fixed to be 3 and 9, respectively. At this step, r, σ and $N^*_{\rm In-Ga}/N^*_{\rm In-In}$ for the type 2 atoms were determined.

Finally, the $E \parallel a$ data were analyzed. In this configuration, all types of atoms contribute to the XAFS signal. The values of r, σ and $N^*_{\rm In-Ga}/N^*_{\rm In-In}$ for the type 1 and 2 atoms, which were obtained from the above two steps, were used. N_1^*, N_2^* and N_3^* were set to be 3, 3 and 6, respectively. All the structural parameters obtained by these fitting methods are summarized in Table 1. Here, $x_{\rm local}$ is the fraction of In atoms around an In atom, which was evaluated using the coordination numbers shown in Table 1.

Table 1
Structural parameters obtained from EXAFS curve-fitting analyses for three types of In—Ga and In—In atomic pairs in the m-plane $In_{0.06}Ga_{0.94}N$ film.

	In—Ga			In—In			
Atomic type	r (Å)	N	σ (Å)	r (Å)	N	σ (Å)	$x_{\rm local}$
No. 1	3.26	5.1	0.09	3.30	0.9	0.10	0.15
No. 2	3.28	3.1	0.07	3.29	0.9	0.06	0.23
No. 3	3.25	1.4	0.07	3.29	0.6	0.07	0.30

For the type 1, 2 and 3 atoms, $x_{\rm local}$ is 0.15, 0.23 and 0.30, respectively. All the values are larger than the InN mole fraction of the film ($x = 0.06$), indicating that a few In atoms are atomically localized in all directions in the m-plane InGaN film. Thus, high internal quantum efficiency due to localized excitons is expected for m-plane InGaN films as is the case of c-plane films.

The Monte Carlo simulation on atomic arrangement in MOVPE-grown InGaN thin films by Kangawa *et al.* shows that In fluctuation in c-plane InGaN films is larger than that in random alloy where In-rich clusters may exist (Kangawa *et al.*, 2007) but that In atoms are scattered on the c-plane (Kangawa *et al.*, 2009). These results suggest that In atoms aggregate along the c-axis, which is consistent with the previous EXAFS results for c-plane InGaN SQWs (Miyanaga *et al.*, 2007). Their simulation also suggests that the distribution of In atoms in a-plane films is almost the same as that in random alloy due to the more sparse distribution of tetrahedral $In_nGa_{4-n}N$ clusters (n = 0, 1, 2, 3, 4) on the a-plane surface than on the c-plane surface. The present In-aggregation in the m-plane InGaN film can be explained by the same mechanism, since tetrahedral clusters are sparsely distributed on the m-plane surface.

The 2NN In—Ga distances in strain-free InGaN crystals are estimated to be 3.23, 3.27 and 3.29 Å for the type 1, 2 and 3 atoms, respectively. These values were calculated using the x_{local} parameters in Table 1 and the lattice constants of GaN (a = 3.1890 Å and c = 5.1864 Å) (Leszczynski *et al.*, 1996) and InN (a = 3.5378 Å and c = 5.7033 Å) (Paszkowicz, 1999) under the virtual-crystal approximation (Mikkelsen Jr & Boyce, 1983). As is expected from the macroscopic compressive strain, the In—Ga distance of the type 2 atoms in the *m*-plane film is elongated and that of the type 3 atoms is shortened, compared with that in strain-free crystals. In contrast, the In—Ga distance of the type 1 atoms is longer than the strain-free value in spite of the compressive strain along the *c*-axis.

This behaviour can be explained by the anisotropy of the atomic structure on the *m*-plane. The *m*-plane film is compressively strained along the *a*- and *c*-axes. By the effect of the compressive strain in the *a*-direction, the In—Ga distances of the type 1 and 2 atoms are elongated and that of the type 3 atoms is shortened, because the first nearest neighbour In—N distance is almost isotropic as mentioned above. On the other hand, compressive strain along the *c*-axis shortens the In—Ga distance of the type 1 atoms and elongates those of the type 2 and 3 atoms. As a result, the two strain effects are partly cancelled for the type 1 and 3 atoms, and it is possible that their atomic distance is longer than the strain-free values even under the compressive strain, depending on the relative magnitude of the two effects. From the present XAFS results, it is found that the effect of the *a*-direction strain is larger than that of the *c*-direction strain. This difference in magnitude between the two effects is considered to be caused by the atomic structure on the *m*-plane, that is, the type 3 atoms and the X atom are on the same plane, whereas the type 1 atoms are *not* on the plane.

It is expected that the local strain around In atoms in coherently grown *m*-plane InGaN films is more relaxed than that in similar *c*-plane films, since the strain effects in *m*-plane films are partly cancelled due to the anisotropic atomic structure as mentioned above. In fact, the atomic distances of in-plane In—Ga and In—In pairs in the *m*-plane film are longer than those in *c*-plane SQWs (∼3.22 Å) (Miyanaga *et al.*, 2007), as seen from Table 1.

4. Conclusion

Polarization-dependent XAFS analyses were carried out for the coherently grown *m*-plane $In_{0.06}Ga_{0.94}N$ film using the step-by-step fitting procedure. From the coordination numbers, a few In atoms were shown to be atomically localized in all directions. The In—Ga distance in the *c*-direction was found to be longer than that in strain-free virtual crystals in spite of the compressive strain along the *a*- and *c*-axes, which can be explained by the partial strain-cancellation mechanism due to the anisotropic atomic structure on the *m*-plane. It was also found that the local strain in coherently grown *m*-plane InGaN is more relaxed than that in coherently grown *c*-plane InGaN.

Acknowledgements

The authors are grateful to S. Mikami for his help with the XAFS measurements. The synchrotron radiation experiments were performed at Photon Factory in KEK under Proposal No. 2007G620.

References

Ankudinov, A. L. & Rehr, J. J. (2000). *Phys. Rev. B*, **62**, 2437–2445.
Bayliss, S. C., Demeester, P., Fletcher, I., Martin, R. W., Middleton, P. G., Moerman, I., O'Donnell, K. P., Sapelkin, A., Trager-Cowan, C., Van Der Stricht, W. & Young, C. (1999). *Mater. Sci. Eng. B*, **59**, 292–297.
Bernardini, F. & Fiorentini, V. (1998). *Phys. Rev. B*, **57**, R9427–R9430.
Blant, A. V., Cheng, T. S., Jeffs, N. J., Foxon, C. T., Bailey, C., Harrison, P. G., Dent, A. J. & Mosselmans, J. F. W. (1997). *Mater. Sci. Eng. B*, **50**, 38–41.
Chichibu, S., Azuhata, T., Sota, T. & Nakamura, S. (1996). *Appl. Phys. Lett.* **69**, 4188–4190.
Chichibu, S. F., Sota, T., Wada, K., Brandt, O., Ploog, K. H., DenBaars, S. P. & Nakamura, S. (2001). *Phys. Status Solidi A*, **183**, 91–98.
Chichibu, S. F., Yamaguchi, H., Zhao, L., Kubota, M., Onuma, T., Okamoto, K. & Ohta, H. (2008). *Appl. Phys. Lett.* **93**, 151908.
Craven, M. D., Waltereit, P., Wu, F., Speck, J. S. & DenBaars, S. P. (2003). *Jpn. J. Appl. Phys.* **42**, L235–L238.
Jeffs, N. J., Blant, A. V., Cheng, T. S., Foxon, C. T., Bailey, C., Harrison, P. G., Mosselmans, J. F. W. & Dent, A. J. (1998). *MRS Proc.* **512**, 519.
Kachkanov, V., O'Donnell, K. P., Martin, R. W., Mosselmans, J. F. W. & Pereira, S. (2006). *Appl. Phys. Lett.* **89**, 101908.
Kangawa, Y., Kakimoto, K., Ito, T. & Koukitu, A. (2007). *Phys. Status Solidi B*, **244**, 1784–1788.
Kangawa, Y., Kakimoto, K., Ito, T. & Koukitu, A. (2009). *J. Cryst. Growth*, **311**, 463–465.
Katsikini, M., Paloura, E. C., Boscherini, F., D'Acapito, F., Lioutas, C. B. & Doppalapudi, D. (2003). *Nucl. Instrum. Methods Phys. Res. B*, **200**, 114–119.
Katsikini, M., Pinakidou, F., Paloura, E. C., Komninou, P., Iliopoulos, E., Adikimenakis, A., Georgakilas, A. & Welter, E. (2008). *Phys. Status Solidi A*, **205**, 2593–2597.
Koida, T., Chichibu, S. F., Sota, T., Craven, M. D., Haskell, B. A. S., Speck, J., DenBaars, S. P. & Nakamura, S. (2004). *Appl. Phys. Lett.* **84**, 3768–3770.
Kuokstis, E., Chen, C. Q., Gaevski, M. E., Sun, W. H., Yang, J. W., Simin, G., Asif Khan, M., Maruska, H. P., Hill, D. W., Chou, M. C., Gallagher, J. J. & Chai, B. (2002). *Appl. Phys. Lett.* **81**, 4130–4132.
Leszczynski, M., Teisseyre, H., Suski, T., Grzegory, I., Bockowski, M., Jun, J., Porowski, S., Pakula, K., Baranowski, J. M., Foxon, C. T. & Cheng, T. S. (1996). *Appl. Phys. Lett.* **69**, 73–75.
Mikkelsen, J. C. Jr & Boyce, J. B. (1983). *Phys. Rev. B*, **28**, 7130–7140.
Miyajima, T., Kudo, Y., Liu, K.-Y., Uruga, T., Asatsuma, T., Hino, T. & Kobayashi, T. (2001). *Phys. Status Solidi B*, **228**, 45–48.
Miyanaga, T., Azuhata, T. S., Matsuda, S., Ishikawa, Y., Sasaki, S., Uruga, T., Tanida, H., Chichibu, S. F. & Sota, T. (2007). *Phys. Rev. B*, **76**, 035314.
Ng, H. M. (2002). *Appl. Phys. Lett.* **80**, 4369–4371.
O'Donnell, K. P., Martin, R. W., White, M. E., Mosselmans, J. F. W. & Guo, Q. (1999). *Phys. Status Solidi B*, **216**, 151–156.
O'Donnell, K. P., Mosselmans, J. F. W., Martin, R. W., Pereira, S. & White, M. E. (2001). *J. Phys. Condens. Matter*, **13**, 6977–6991.
Onuma, T., Chakraborty, A., Haskell, B. A., Keller, S., DenBaars, S. P., Speck, J. S., Nakamura, S., Mishra, U. K., Sota, T. & Chichibu, S. F. (2005). *Appl. Phys. Lett.* **86**, 151918.

Paszkowicz, W. (1999). *Powder Diffr.* **14**, 258–260.
Sakane, H., Miyanaga, T., Watanabe, I., Matsubayashi, N., Ikeda, S. & Yokoyama, Y. (1993). *Jpn. J. Appl. Phys.* **32**, 4641–4647.
Sasaki, S., Miyanaga, T., Azuhata, T., Uruga, T., Tanida, H., Chichibu, S. F. & Sota, T. (2007). *AIP Conf. Proc.* **882**, 499–501.
Takeuchi, T., Sota, S., Katsuragawa, M., Komori, M., Takeuchi, H., Amano, H. & Akasaki, I. (1997). *Jpn. J. Appl. Phys.* **36**, L382–L385.
Waltereit, P., Brandt, O., Trampert, A., Grahn, H. T., Menniger, J., Ramsteiner, M., Reiche, M. & Ploog, K. H. (2000). *Nature (London)*, **406**, 865–868.